Springer

KSME

Journal of Mechanical Science and Technology 24 (7) (2010) 1545~1551
www.springerlink.com/content/1738-494x
DOI 10.1007/s12206-010-0407-3

Theoretical and numerical analyses of a ceramic monolith heat exchanger †

Jin Gi Paeng[1], Young Hwan Yoon[2,*], Kyung Hwan Kim[3] and Keon Sik Yoon[4]

[1]*School of Mechanical and Aerospace Engineering, Gyeongsang National University, Jinju, 660-701, Korea*
[2]*Department of Mechanical Engineering, Changwon National University, Changwon, 641-773, Korea*
[3]*Division of Facilities, Changwon National University, Changwon, 641-773, Korea*
[4]*Department of Naval Architecture and Marine Engineering, Changwon National University, Changwon, 641-773, Korea*

(Manuscript Received December 7, 2009; Revised February 8, 2010; Accepted March 30, 2010)

Abstract

This study assessed the performance of a ceramic monolith heat exchanger, estimating heat transfer and pressure drop by numerical computation and the ε-NTU method. A heat exchanger consists of rectangular ducts for exhaust gas, a ceramic core, and rectangular ducts for air and exhaust gases, as well as air in the cross-flow direction. The numerical computations were performed for the whole domain, including the exhaust gas, ceramic core, and air. In addition, the heat exchanger was examined using a conventional ε- NTU method with several Nusselt number correlations from the literature to characterize the flow in the rectangular duct. The results of these numerical computation analyses demonstrated that the effectiveness of the heat exchanger, as demonstrated using the ε-NTU method with Stephan's Nusselt number correlation, came closest to the results of computation with a relative error of 2%. The air-side pressure drops indicated by the results of numerical computation were 13-22% higher than those calculated using the head loss equation with the inclusion of a friction factor that was obtained from previous experiments examining heat transfer conditions.

Keywords: Ceramic recuperator; Conjugate heat transfer; Cross flow; Effectiveness; HRU; Pressure drop

1. Introduction

World energy consumption demands are steadily growing due to increases in industrial production and population. However, the fossil fuels that are most readily available cause environmental pollution and will be exhausted in the near future. Therefore, fuel cell systems are gaining popularity in the world energy market as a source of alternative energy.

Solid oxide fuel cells (SOFC) of various types are capable of upwards of 60% electric conversion efficiency. However, they produce high exhaust gas temperatures of 600-1000℃ and require recuperators to recover this thermal energy, which would otherwise be wasted. Accordingly, heat resistant material is necessary for the construction of high temperature heat exchangers. The recovered heat may be used to generate electricity in SOFC/GT hybrid power generating systems including gas turbines and HRU (heat recovery system), as shown in Fig. 1 [1]. Recently, a hybrid recuperator has been considered for use in such power systems. Hybrid recuperators consist of three pass recuperators (Fig. 2 [1]): the first is a ceramic heat exchanger with a working temperature between 600℃ and 1,000℃ and the second and the third are metallic heat exchangers with working temperatures under 600℃. For a sense of perspective, the working temperatures of heat exchangers for general use are normally less than 150℃.

Numerous studies have been conducted examining the performance of recuperators. The focus of most of these has been the improvement of overall system efficiency. Rokni and Sunden [2] simulated turbulent gas flow and heat transfer in ducts with different cross-sectional measurements using a different turbulence model, implementing the use of thermal boundary conditions-either constant temperature or constant heat flux-on all of the walls. Ranganayakulu et al. [3] investigated the combined effects of longitudinal heat conduction, inlet flow non-uniformity, and temperature non-uniformity on thermal performance in a cross-flow plate heat exchanger. Hetsroni et al. [4] conducted experiments on channel heat transfer, finding that flow instabilities caused pressure fluctuation which decreased the heat transfer rate. Bourisa et al. [5] modified a tube bundle heat exchanger in order to achieve a higher heat transfer capability. In this particular study, the optimized tube shape among three different cross sections was determined after the efficiency of the corresponding recuperators was compared and simulated. Tsuzuki et al. [6] studied a three dimensional thermal-hydraulic simulation of a printed circuit heat exchanger by applying the computer code,

† This paper was recommended for publication in revised form by Associate Editor Ji Hwan Jeong

*Corresponding author. Tel.: +82 55 279 7501, Fax: +82 55 275 0101
E-mail address: yhyoon@changwon.ac.kr

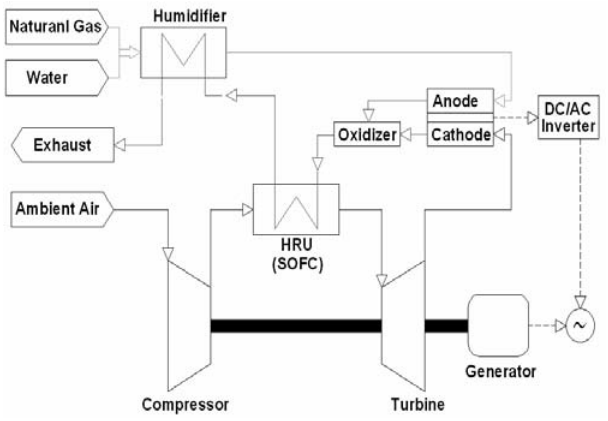

Fig. 1. Schematic of SOFC/GT hybrid power generating system.

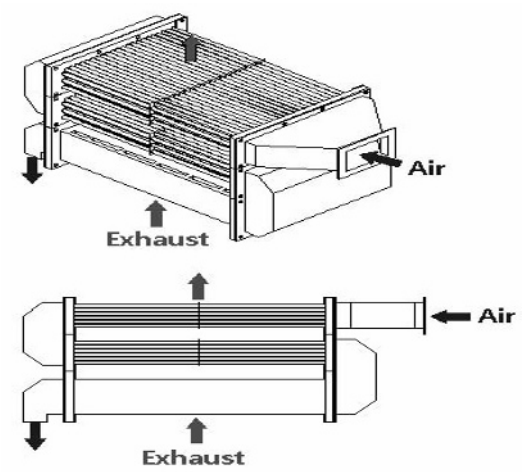

Fig. 2. Schematic of a three pass recuperator.

FLUENT. The optimized flow channel design was accomplished by changing the fin shape and angle to reduce the pressure drop and increase heat transfer performance. Park et al. [7] designed a highly efficient ceramic exchanger for their research focusing on a theoretical analysis, performing a CFD simulation. The numerical computation was performed using a simple rectangular fin-type model.

Most of these research papers computed the heat transfer characteristics for a single passage or tube bundle of the fluid flows [2-7]. However, in this paper, we conducted computational conjugate numerical analyses of the heat transfer for a monolithic whole heat exchanger with rectangular channels [8]. Furthermore, the heat transfer rate was also evaluated using the ε-NTU theoretical method, using various Nusselt number correlations for comparison with the numerical computation.

Ceramic heat exchangers offer the benefits of cheap material costs, but suffer from low thermal efficiency compared to metallic heat exchangers. In this study, the performance of a ceramic heat exchanger including three pass recuperators was analyzed so as to predict performance, heat transfer rate, effectiveness, and pressure drop.

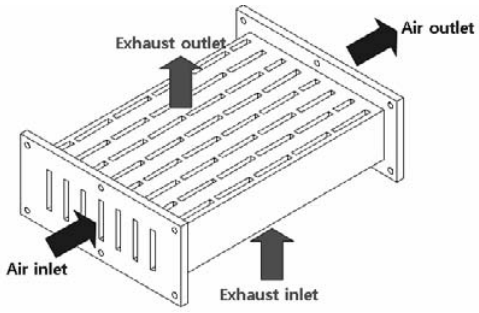

Fig. 3. Schematic drawing of the ceramic heat exchanger.

2. Theory

2.1 Design and analysis model of ceramic recuperator

The ceramic recuperator consists of a rectangular hot exhaust and cold air passages with the exhaust and air passing in the cross-flow direction without mixing with each other (Fig. 3).

2.2 Overall heat transfer coefficient of the ceramic heat exchanger

The overall heat transfer coefficient, U, between hot and cold fluids is a principal factor in estimating the rate of heat transfer. It is expressed as Eq. (1) [8].

$$U = \frac{1}{\frac{1}{h_{air}} + \frac{\Delta X}{k} + \frac{A_{air}}{\eta_t A_{gas} h_{gas}}} \tag{1}$$

Here k is thermal conductivity of the ceramic core, $\triangle X$ is the thickness of the wall, and A_{air} and A_{gas} are the air-side and the exhaust-side heat transfer areas, and h_{air} and h_{gas} are also each side average convective heat transfer coefficients, which are obtained from Nusselt relation of Eq. (2). In addition, η_t is the total surface effectiveness of a fin.

$$h = Nu \times \frac{k}{D_h} \tag{2}$$

k of above equation is thermal conductivity of each fluid and D_h is a hydraulic diameter of the rectangular fluid passage. Correlation equations of the Nusselt number from literature are listed in Table 1. The equations in Table 1 were derived under fully developed or developing flow conditions with constant wall heat transfer rate (q''=const).

2.3 ε -NTU Method

The thermal performance of the ceramic heat exchanger was calculated using a theoretical equation of the *ε -NTU* method in which the effectiveness (ε) is expressed as Eq. (3) for an unmixed fluid flow condition [8]. These results were then compared to the numerical computation.

$$\xi = 1 - \exp\left\{\frac{NTU^{0.22}}{C}\left[\exp\left(-CNTU^{0.78}\right) - 1\right]\right\} \tag{3}$$

Here C represents the ratio of heat capacity (C_{min}/C_{max}). *NTU*

Table 1. Correlations of Nusselt numbers in ducts as reported in the literature.

Reference	Correlation	Conditions		Range of validity
		Geometry	Flow regime	
Kays and Crawford [9]	Nu=8.235(1-1.883/ α +3.767/ α^2 -5.814/ α^3 +5.361/ α^4 -2/ α^5	Retangular	Fully developed (constant Wall heat flux)	Re < 2200
Sieder-Tate correlation [10]	$Nu=1.86(RePrD_h/L)^{1/3}\left(\frac{\mu_f}{\mu_\omega}\right)^{0.14}$	Circular	Simultaneously developing (constant wall temperature)	Re < 2200
Stephan correlation [11]	$Nu=4.364+\frac{0.086(RePrD_h/L)^{1.33}}{1+0.1\Pr(ReD_h/L)^{0.83}}$	Circular	Simultaneously developing Simultaneously developing (constant wall temperature)	$0.7<Pr<7$ or $RePrD/L<33$ (*for* $Pr>7$)
Shah and London [12]	$Nu=\begin{cases}1.953(RePrD_h/L)^{1/3}\\4.364+0.0722(RePrD_h/L)\end{cases}$	Circular	Thermally developing laminar (constant wall temperature)	$RePrD/L\geq 33$ $RePrD/L<33$

is defined by the total conductance (UA) divided by the minimum heat capacity (C_{min}), where C_{min} is the lower heat capacity $(\dot{m}c_p)_{\min}$ and C_{max} is the higher heat capacity $(\dot{m}c_p)_{\max}$ of the two fluids where $\dot{m}$ and c_p are the mass flow rate and specific heat of the hot and cold fluids, respectively. Subsequently, the rate of heat transfer from hot to cold fluids can be computed as Eq. (4).

$$q=\varepsilon\times C_{\min}(T_{gas\_in}-T_{air\_in}) \tag{4}$$

Then the outlet temperatures of exhaust and air (T_{air_out} and T_{gas_out}) are evaluated with the inlet temperatures of both fluids as Eq. (5) and Eq. (6).

$$T_{air\_out}=T_{air\_in}+\frac{q}{c_{p\_air}} \tag{5}$$

$$T_{gas\_out}=T_{gas\_in}+\frac{q}{c_{p\_gas}} \tag{6}$$

2.4 Pressure drop

Pressure drop is a major factor in rating a heat exchanger's heat transfer capabilities. The Darcy friction equation for pressure drop is as follows (Eq. (7)) [8].

$$\Delta P_{core}=f\frac{1}{2}\rho_m V_m^2(L/D_h) \tag{7}$$

Here $f=\frac{64}{\mathrm{Re}}$ since the flow in this paper was considered to be laminar.

3. Numerical analysis

There are few experimental data concerning the thermal performance of ceramic monolith heat exchangers. Therefore, numerical computations were necessary in order to assess the performance of the heat exchanger tested in this study. These were performed by computing conjugated heat transfers through the whole domain, including the fluid and ceramic solid region.

3.1 Governing equations

For the computations, the fluid flows were assumed to be three-dimensional, incompressible, and of a steady state. All of the fluid flows for both cold fluid and hot exhaust were assumed to be laminar, since the Reynolds number is less than 2,300. The governing equations for the steady state and laminar flow were written as:

Continuity equation :

$$\frac{\partial}{\partial x_j}(\rho u_j)=0 \tag{8}$$

Momentum equation :

$$\frac{\partial}{\partial x_j}(\rho u_j u_i)=-\frac{\partial P}{\partial x_i}+\frac{\partial \tau_{ij}}{\partial x_j} \tag{9}$$

Here p : static pressure

$\tau_{ij}=\left[\mu\left(\frac{\partial u_i}{\partial x_j}+\frac{\partial u_j}{\partial x_i}\right)\right]-\frac{2}{3}\mu\frac{\partial u_i}{\partial x_j}\delta_{ij}$: stress tensor

Energy equation :

$$\rho c_p\frac{\partial}{\partial x_j}(u_j T)=k\frac{\partial^2 T}{\partial x_j^2} \tag{10}$$

3.2 Computational grid

The ceramic heat exchanger that we tested is shown, with its dimensions, in Fig. 4. The numerical analysis domain includes half of the heat exchanger, shown in the figure as a red line, since the heat exchanger is symmetrical. The total dimensions of the numerical model were 305.5×497.5×65 mm^3. Fig. 5 presents the computational grids determined by GAMBIT V2.3 [13], meshing approximately 800,000 cells of a hexahedron. This computation was done using FLUENT V6.2 commercial software with a finite volume method and simple algorithm [13].

In order to evaluate the sensitivity of the cell number, the number of cells was increased from 200,000 to 800,000 (Fig. 6). We observed less than 0.3% error between the air side pressure drop with 700,000 cell numbers and that with 800,000. Therefore, the cell size was determined to be

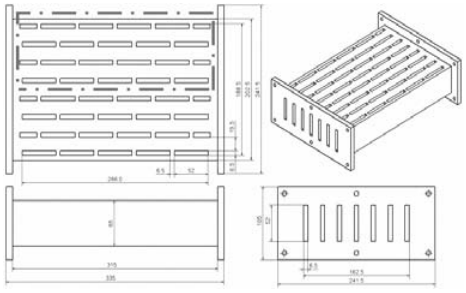

Fig. 4. A representation of the ceramic exchanger core with its dimensions.

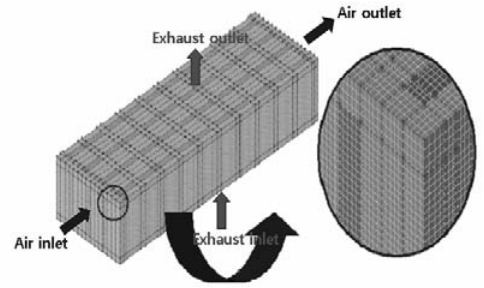

Fig. 5. A schematic drawing of the ceramic heat exchanger.

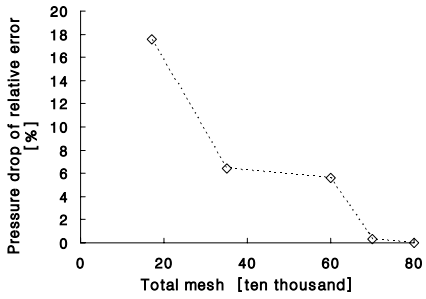

Fig. 6. Sensitivity of mesh grid.

800,000 for all of the numerical computations in this study.

3.3 Boundary conditions

In this computation, a principal velocity profile at each inlet was assigned as uniform according to the mass flow rate, but the two velocity components perpendicular to the principal directions were assumed to be zero. The temperature was also assumed to be uniform, at inlet as Eq. (11).

$$T = T_{in} \tag{11}$$

Atmospheric pressure was given at each exit for the flow passages, since the exits are open to the atmosphere. For the boundary conditions of temperature at the exits, adiabatic conditions were imposed (as Eq. (12)).

$$\frac{\partial T}{\partial x_i} = 0 \tag{12}$$

Non-slip conditions were applied on the walls of all fluid flows (as Eq. (13)). Adiabatic conditions were imposed at the outer walls of the ceramic core, except for the walls of the flow passages for cold air and hot exhaust (as Eq. (12)).

$$U_{wall} = V_{wall} = W_{wall} = 0 \tag{13}$$

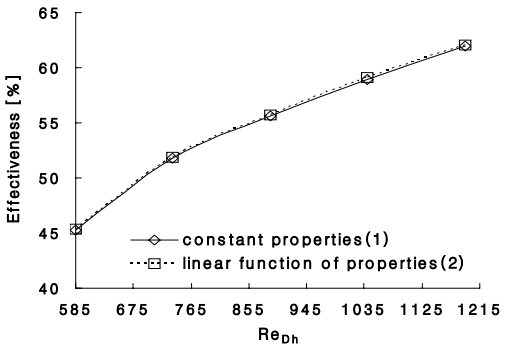

Fig. 7. Comparison between solutions with constant properties and the linear function of the properties.

4. Results

The numerical computations of the heat transfer characteristics for the ceramic heat exchanger were compared to theoretical calculations of heat transfer assuming various Nusselt number correlations in Table 1.

4.1 Computational results

Before computations of problem, the thermodynamic properties of the heat exchanger were tested by assuming that, for two ways, one has constant properties at average temperature for both inlet and outlet and the other one is a linear function to the fluid temperature. Fig. 7 shows the computations for these two thermodynamic properties assumptions. In this figure, the two results (dotted and solid lines) are close to each other, with the relative errors of 0.1 to 0.22%. Therefore, the thermodynamic properties were assumed to be constant with an average fluid temperature.

For reference, Table 2 [8] presents the air properties at 631℃ and the exhaust properties at 787℃. Table 3 [14] also presents the properties of the ceramic core made silicon carbide (SiC) that were assumed for the purposes of numerical computation.

The numerical computations were carried out for the exhaust mass flow rate of 0.001983 kg/s, varying the air flow rate from 0.001983 kg/s to 0.003966 kg/s in five steps. The Reynolds numbers according to the mass flow rates are presented in Table 4. All Reynolds numbers are based on mean temperatures of inlet and outlet temperatures.

For instance, Fig. 8 presents the contours of the temperature distribution of the air (a) and exhaust gas (b) assuming an air-side Reynolds number of 585 and a gas-side Reynolds number of 79, which indicates that the mass flow rates of the air and the exhaust were the same at 0.001983 kg/s (Table 4). The air (a) flows from the left side to the right side, so the air tempera-

Table 2. Fluid properties for CFD analysis (Re_{Dh}=585).

Properties	Air side	Exhaust side
	Mean temperature 631 [℃]	Mean temperature 631 [℃]
ρ [kg / m^3]	0.391	0.340
c_p [J / kgK]	1111.7	1138.7
k [W / mK]	0.062	0.070
μ [kg / ms]	3.875×10^{-5}	4.300×10^{-5}

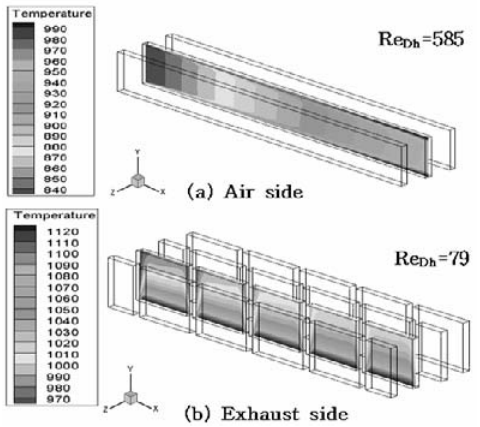

Fig. 8. Contours of temperature distributions of air (a) and exhaust (b) flows [unit: K].

ture increases, moving from the left inlet to the right exit. In contrast, the exhaust gas (b) flows from the bottom to top so that the temperature is cooled from the high inlet temperature to the low exit temperature. Furthermore, Fig. 9 presents the temperature profiles of the ceramic core under these conditions. The temperature increased from the left end to the right end of the heat exchanger as the air temperature increased from the left inlet to the right exit.

4.2 Computation of the numerical and theoretical results

For a theoretical calculation of heat transfer, the total heat transfer coefficient, U, between the hot exhaust and cold air should be evaluated assuming various Nusselt number correlations (e.g. as in Eq. (1) and Table 1). Fig. 10 shows four lines of the total heat transfer coefficient from the Nusselt number correlations of Kays and Crawford [9], Sieder and Tate [10], Stephan [11], and Shah and London [12]. In this figure, the total heat transfer coefficient calcuated by Kays and Crawford is the highest and is invariant regardless of Reynolds number, since the correlation is realized under fully developed flow conditions. All of the other lines increased towards the Reynolds number, because they are under developing flow condition.

The effectiveness of a ceramic heat exchanger is defined as the actual heat transfer rate over the maximum possible heat transfer rate, as (Eq. (14)):

$$\varepsilon = \frac{C_h(T_{gas\_in} - T_{gas\_out})}{C_{\min}(T_{gas\_in} - T_{air\_in})} = \frac{C_C(T_{air\_out} - T_{air\_in})}{C_{\min}(T_{gas\_in} - T_{air\_in})} \quad (14)$$

Here C_h and C_C are heat capacity rates of gas and air, respectively.

Table 3. Thermodynamic properties of ceramic core (Temperature : 400 ℃).

Properties	Ceramic core
ρ [kg / m^3]	3100
c_p [J / kgK]	670
k [W / mK]	77.5

Table 4. Mass flow rates according to Reynolds number (under conditions of fixed exhaust flow).

Air side		Exhaust side	
Re_{Dh}	$\dot{m}_{sir}$ [kg / s]	Re_{Dh}	$\dot{m}_{gas}$ [kg / s]
585	0.001983	79	0.001983
736	0.002479		
888	0.002975		
1040	0.003471		
1192	0.003966		

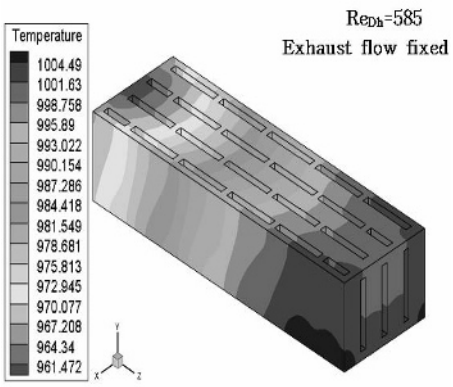

Fig. 9. Contours of temperature distributions of ceramic core [unit: K].

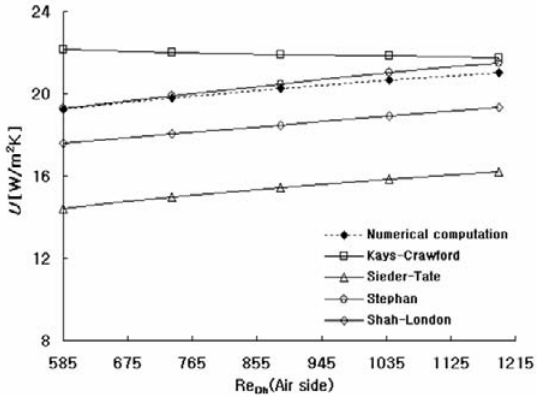

Fig. 10. Comparison of overall heat transfer coefficient with various correlations of Nusselt numbers (gas side Reynolds number :79).

Fig. 11 presents a comparison between the effectiveness of the numerical computation (dotted line) and the effectiveness of the theoretical equation (solid line), derived using Eq. (3) assuming various Nusselt number correlations. From this figure, the deviations of the theoretical effectiveness were 2.8-7.2% for Kays and Crawford [9], 13.0-14.4% for Sieder and

Table 5. Comparison of outlet fluid temperatures between numerical computation and ε-NTU method.

Re_{Dh}	Air side temperature [℃]			Exhaust side temperature [℃]		
	Inlet	Outlet		Inlet	Outlet	
		Numerical computation	ξ -NTU		Numerical computation	ξ -NTU
585	560	700	693	850	722	721
1192	560	652	642	850	695	691

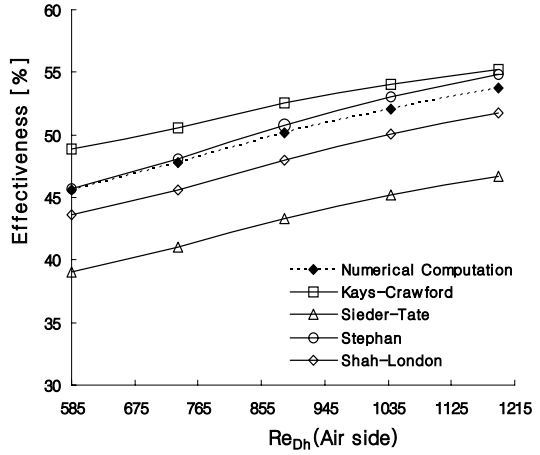

Fig. 11. Comparison of the effectiveness between the numerical computation and ε-NTU method with various correlations of the Nusselt number (gas side Reynolds number: 79).

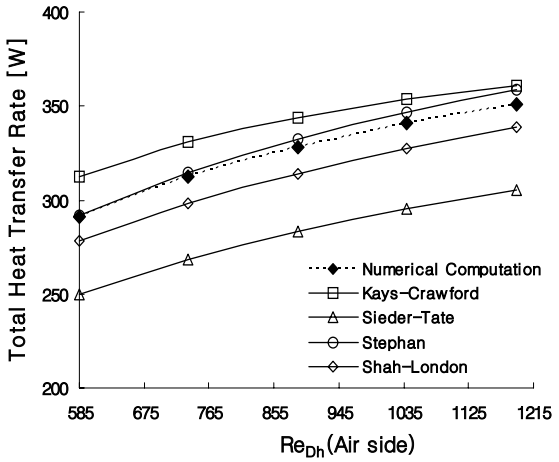

Fig. 12. Comparison of the total heat transfer from the numerical computation and ε-NTU method (gas side Reynolds number: 79).

Tate [10], 0.25-2.14% for Stephan [11], and 3.5-4.6% for Shah and London [12] to the effectiveness by the numerical computation, respectively. The largest error was 14.4%; however, the Stephan's correlation (circle marks) was the closest to that by the numerical computation (dotted line).

The total heat transfer rate of the ceramic heat exchanger is plotted in Fig. 12 in the same manner. This figure shows almost the same trend to effectiveness in Fig. 11, since the total heat transfer rate is proportional to the effectiveness under the same conditions.

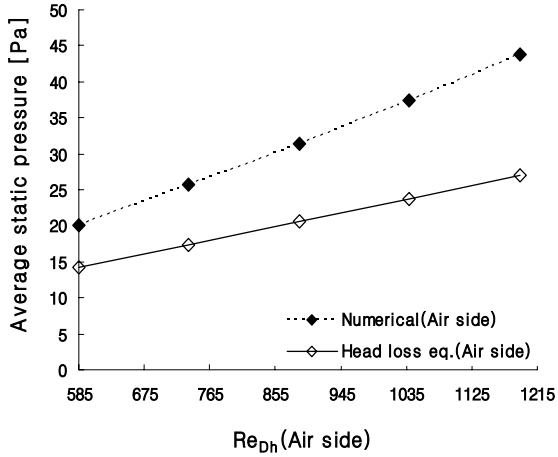

Fig. 13. Comparison of air side pressure drop from numerical computation and head loss equation according to Reynolds number.

The exit temperatures of each fluid are provided in Table 5, and were obtained by numerical computation and the ε-NTU method assuming a smallest Reynolds number of 585 and a largest Reynolds number of 1192. The relative error between the exit temperatures from the numerical computation and ε-NTU method was less than 0.44% for the exhaust and less than 1.15% for the air.

Fig. 13 shows two lines describing the air side pressure drop: a dotted line obtained from the numerical computation, a solid line calculated using a head loss equation with the inclusion of a friction factor (Eq. (7)). As shown in figure, the pressure drop indicated by the numerical computation with heat transfer was higher, up to 29-38%, for the reference of the numerical computation, than that by head loss equation with the inclusion of a friction factor. We calculated the length of entrance region for fully developed flow in the air side passages such that $L_h=0.05Re_hD_h$=0.34-0.7 m. However, the full length of air passage is only 0.315m. Therefore, it can be said that the full length of air passage was under developing flow condition. The difference may be explained by the fact the fluid flow according to the numerical computation is under developing flow conditions from the uniform inlet velocity profile. In the other hand, head loss equation with the inclusion of a friction factor is under fully developed fluid flow conditions, which produces a lower pressure drop relative to developing flow.

5. Conclusions

In this study, numerical computations were carried out for the hot exhaust, ceramic core, and cold air areas in a ceramic heat exchanger measuring 800-1,000℃. The effectiveness and the total heat transfer rates as calculated by numerical computation were compared with those derived using a ε-NTU method assuming various Nusselt number correlations drawn from the current literature.

(1) The relative errors of the total heat transfer as calculated by the ε-NTU method using five Nusselt number correlations

drawn from the literature were less than 14.4% versus those calculated by numerical computation. Among the Nusselt number correlations, the total heat transfer results calculated by the ε-NTU method with Stephan's correlation was closest to those of numerical computation.

(2) Accordingly, the exit temperature calculated by the ε-NTU method with Stephan's correlation was simulated within 1.15% of the relative error for the exhaust exit temperature and 0.44% for the air exit temperature calculated by numerical computation.

(3) Air-side pressure drops calculated by numerical computation were 29~38% higher, for the reference of the numerical computation, than those calculated using the head loss equation with the inclusion of a friction factor.

Acknowledgment

This work was financially supported by the Ministry of Education and Human Resources Development (MOE), the Ministry of Commerce, Industry and Energy (MOCIE) and the Ministry of Labor (MOLAB) through the fostering project of the Industrial-Academic Cooperation Centered University.

This work was additionally supported in its second phase by the Bk21 Project.

Nomenclature

C : Ratio of capacity
D_h : Hydraulic diameter
h : Heat transfer coefficient
k : Thermal conductivity
L : Heat exchanger length
Nu : Nusselt number
P : Static pressure
Pr : Prandt number
U : Overall heat transfer coefficient
u : Velocity
α : Aspect ratio of channel
ρ : Density
μ : Viscosity
δ_{ij} : Kronecker delta
x_i : Cartesian coordinate
ε : Effectiveness

References

[1] N. Bessette, D. S. Schmitt, J. Rawson and L. Allfather, Fuel transformer, *Technical Progress Report Semi Annual, Acumentircs Practice*, 13 (6) (2005) 789-803.

[2] M. Rokni and B. Snden, A numerical investigation of turbulent force convection in ducts with rectangular and trapezoidal cross-section area by using different turbulence models. *Numerical Heat Transfer,* 30 (1996) 321-346.

[3] C. Ranganayakulu and N. K. Seetharamu, The Combined Effects of Wall Longitudinal Heat Conduction, Internal Fluid Flow Non-uniformity and Temperature Non-uniformity in Compact Tube-Fin Heat Exchangers, *Int. J. Heat and Mass Transfer,* 42 (1996) 263-273.

[4] G. Hetsroni, A. Mosyak, Z. Segal and G. Ziskind, A Uniform Temperature Hot Sink for Cooling of Electronic Device, *Int, J. Heat Mass Transfer,* 45 (2002) 3275-3286.

[5] D. Bourisa, E. Konstantinidisa, S. Balabanib, D. Castigliab and G. Bergeles, Design of a Novel Intensified Heat Exchanger for Reduced Fouling Rates, *Int. J. Heat and Mass Transfer,* 48 (18) (2005) 318-3822.

[6] N. Tsuzuki, Y. Katoa and T. Ishiduka, High Performance Printed Circuit Heat Exchanger, *Applied Thermal Eng,* 27 (10) (2007) 1702-1707.

[7] S. K. Park, G.C. Choi, H. J. Nam, H. D. Shin and H. S. Park, A Numerical simulation for Design of High Temperature Ceramic Heat Exchanger, *The Korean Society of Combustion,* 3 (2009) 24-28.

[8] F. A. Mill, *Basic Heat and Mass transfer*, 2nd ed Prentice Hall, New Jersey, (2003) 687-689.

[9] M. W. Kays and M. E. Crawford, *Convective heat and mass transfer*, McGraw Hill, New York, (1980).

[10] P. F. Incropera, and D. P. Dewitt, *Fundamentals of heat and mass transfer*, John Wiley and Sons, New York. Publishing Company, New York, USA, (1992).

[11] K. Stephan and P. Preußer, Wärmeübergang und maximale Wärmestromdichte beim behältersieden binärer und ternärer flüssigkeitsgemische, *Chem. Ing* 51 (1979) 37.

[12] K. R. Shah and A. L. London, Laminar flow forced convection in duct, *Supply 1, Adv. Heat transfer,* (1978).

[13] FLUENT 6.2 User's Guide, Lebanon, NH, Fluent Inc, (2003).

[14] *Automation Creations. Inc*, http://www.matweb.com.

Young-Hwan Yoon received his Ph. D in Mechanical Engineering from University of Iowa, U.S.A., in 1983. He is a Professor in the Department of Mechanical Engineering at Changwon National University, Changwon,, Korea. His main research interests are compact heat exchanger, numerical heat transfer, and air conditioning system. Currently, he is working on ceramic and metallic heat exchanger for heat recovery unit, coal drying system, and thermoelectric cooling system.

Jin-Gi Paeng received his Ph.D in Mechanical Engineering from Chang-won National University, Changwon, Korea, in 2008. He is currently a research associate in the Department of Aerospace Engineering at Gyeongsang National University, Korea. His research interests are numerical heat transfer, FSI and FSW.